Shroom3-mediated recruitment of Rho kinases to the apical cell junctions regulates epithelial and neuroepithelial planar remodeling

Tamako Nishimura and Masatoshi Takeichi*

Remodeling of epithelial sheets plays important roles in animal morphogenesis. Shroom3 is known to regulate the apical constriction of epithelial cells. Here, we show that Shroom3 binds ROCKs and recruits them to the epithelial apical junctions. We identified the Shroom3-binding site (RII-C1) on ROCKs, and found that RII-C1 could antagonize the Shroom3-ROCK interaction, interfering with the action of Shroom3 on cell morphology. In the invaginating neural plate/tube, Shroom3 colocalized with ROCKs at the apical junctions; Shroom3 depletion or RII-C1 expression in the tube removed these apically localized ROCKs, and concomitantly blocked neural tube closure. Closing neural plate exhibited peculiar cell assemblies, including rosette formation, as well as a planar-polarized distribution of phosphorylated myosin regulatory light chain, but these were abolished by ROCK inhibition or RII-C1 expression. These results demonstrate that the Shroom3-ROCK interaction is crucial for the regulation of epithelial and neuroepithelial cell arrangement and remodeling.

KEY WORDS: Shroom, Rho kinase, Myosin, Neural tube, Epithelial remodeling, Chicken, MDCK cells, Mouse

INTRODUCTION

During embryonic development, epithelial cell layers undergo a variety of dynamic morphological changes, such as folding, invagination and elongation, to generate the tissues with complex architecture. At the cellular level, these processes involve cell intercalation and migration, as well as the apical constriction of epithelial layers (Pilot and Lecuit, 2005). It is thus crucial to understand the mechanisms governing the regulation of these cell behaviors at the appropriate times and locations during development.

Apical constriction occurs in many morphogenetic processes, including gastrulation and neurulation (Lecuit and Lenne, 2007). In epithelial layers, the zonula adherens or adhesion belt, which represents a form of the cadherin-based adherens junction, encloses the cells near the apical end of their lateral cell-cell contacts (Perez-Moreno et al., 2003; Tepass et al., 2001), organizing the apical junctional complex (AJC) together with the tight junctions and desmosomes (Farquhar and Palade, 1963; Vogelmann and Nelson, 2005). F-actin assembles at the cytoplasmic side of the adhesion belt, and its contraction is thought to be a major mechanism for the apical constriction of epithelial layers. When this occurs in embryonic cells, the cells assume a wedge-like shape. This shape change is often used to force epithelial sheets to invaginate. Apical constriction signals for *Drosophila* mesodermal invagination have been extensively studied (Lecuit and Lenne, 2007): upon the binding of an apically secreted ligand, Fog, to its receptors, $G\alpha_{12/13}$-Corcentina is activated (Costa et al., 1994; Parks and Wieschaus, 1991); subsequently, RhoGEF2 becomes activated and anchored to the apical membranes via its interaction with the transmembrane protein T48 (Barrett et al., 1997; Kolsch et al., 2007; Nikolaidou and Barrett, 2004; Rogers et al., 2004). These processes seem to induce

the activation of Rho1 and Rho kinase at the apical cell junction, which in turn leads to the invagination of the future mesodermal layer.

In vertebrates, Shroom3, an actin-binding protein, is known to be a key player for epithelial apical constriction. Shroom3 has been identified as a gene product whose mutation disrupts neurulation (Copp et al., 2003; Hildebrand and Soriano, 1999). This protein is localized at the AJC of the neural tube; and its depletion causes neural tube closure defects in mice and *Xenopus* (Haigo et al., 2003; Hildebrand and Soriano, 1999). When Shoom3 is overexpressed in epithelial cells, it induces their apical constriction along with increased accumulation of myosin 2 (Haigo et al., 2003; Hildebrand, 2005). Shroom3 was also reported to recruit γ-tubulin to the apical areas in the *Xenopus* neural tube (Lee et al., 2007). Shroom3 belongs to the Shroom family, which includes structurally related molecules, Shroom1, Shroom2 and Shroom4 (Hagens et al., 2006), each of which shows unique functions (Dietz et al., 2006; Fairbank et al., 2006; Hagens et al., 2006; Lee et al., 2007; Yoder and Hildebrand, 2007). Shroom family members share similarity in several domains, each having a PDZ domain, to Apx/Shrm-specific domains called ASD1 and ASD2, and putative EVH1- and PDZ-binding sites (Hildebrand and Soriano, 1999); and all the members have the ASD2 domain in common (Hagens et al., 2006). The ASD2 domain of Shroom3 has been shown to be essential for its apical constriction activity (Dietz et al., 2006); however, how this domain acts has yet to be understood.

Previous studies showed that the action of Shroom3 on epithelial constriction required Rho kinases (ROCKs) and myosin 2 (Hildebrand, 2005), but how these molecular systems work together remains unknown. In the present study, we show that Shroom3 physically associated with the ROCKs via the ASD2 domain, and recruited them to the apical junctions in epithelial cell lines, as well as in the chicken neural tube. ROCKs are Ser/Thr kinases, which are activated by binding to the GTP-bound form of RhoA (Riento and Ridley, 2003). Myosin regulatory light chain (MLC) is one of the targets phosphorylated by ROCKs. Phosphorylation of MLC activates myosin 2, leading to the

RIKEN Center for Developmental Biology, 2-2-3 Minatojima-Minamimachi, Chuo-ku, Kobe 650-0047, Japan.

*Author for correspondence (e-mail: takeichi@cdb.riken.jp)

actomyosin contraction (Matsumura, 2005). ROCKs phosphorylate the MLC directly (Amano et al., 1996) and also indirectly, for ROCKs also phosphorylate and inactivate the MLC phosphatase (Kawano et al., 1999). Although ROCKs are mainly cytoplasmic, some of them localize at cell-cell junctions and regulate the assembly of tight (Walsh et al., 2001) or adherens (Sahai and Marshall, 2002) junctions. ROCKs have also been reported to be expressed in the neural plate and involved in neurulation in the chicken embryo (Wei et al., 2001). The results obtained in this present study suggest that the main function of Shroom3 is to recruit ROCKs to the apical junctions, so that Shroom3 can induce their constriction. We also show a peculiar arrangement of neuroepithelial cells and unique distribution of phosphorylated MLC in the closing neural tube, which may explain the cellular basis of its bending mechanisms.

MATERIALS AND METHODS
Expression plasmids and recombinant proteins
Expression plasmid for mouse Shroom3 was kindly provided by P. Soriano. Full-length Shroom3 and its deletion mutants were subcloned into the pCA vector with a FLAG-tag sequence on its 5′ end. For tetracycline-dependent expression, cDNAs for FLAG-tagged Shroom3 and its deletion mutants were subcloned into pTRE2hyg vector (BD Biosciences). Complementary DNAs for Rock1 and Rock2 (also known as ROCK-I and ROCK-II) were obtained by PCR using a mouse Marathon-Ready cDNA library (Clontech), and subcloned into the pCA-HA vector. RNAi vectors for chicken Shroom3 were generated by inserting annealed oligonucleotides for target sequences into the *Bam*HI-*Hin*dIII site of the pSilencer-U6-neo vector (Ambion). The target sequences are as follow: Shrm RNAi, 5′-AAGTCTACTTAAG-CATGTCAA-3′; control RNAi, 5′-AATCACGATGAATGTACTATC-3′. Partial cDNA for chicken Shroom3 (amino acids 503 to 1130) was obtained by amplifying a cDNA library from E1.5 chicken embryos and subcloned into the pCA vector with an EGFP sequence on its 5′ end.

Bacterial expression plasmids for glutathione S-transferase (GST)-tagged proteins were constructed by using the pGEX-4T vector (GE Healthcare). Tagged recombinant proteins were expressed in *E. coli* and purified by use of glutathione-Sepharose beads (GE Healthcare).

Antibodies
The cDNA fragments encoding amino acids 195-423 of mouse Shroom3, 562-836 of mouse Rock1 and 482-838 of chicken Rock1 were cloned into the pGEX-4T vector. The antigens were expressed and purified as above. Antibodies against mouse Shroom3 were generated by immunizing rabbits; and those to mouse Rock1 and chicken Rock1 were raised by immunizing rats. All antibodies were affinity purified by use of antigen-coupled CH-Sepharose beads (GE Healthcare). The specificity of each antibody was confirmed by western blotting (see Fig. S5 in the supplementary material). The following antibodies were purchased: mouse anti-Rock1 and anti-Rock2 (BD Biosciences); mouse anti-phospho-myosin light chain (Ser19, Cell Signaling); mouse anti-ZO-1, rabbit anti-ZO-1 and mouse anti-Lamin B1 (Zymed); mouse anti-α-tubulin clone DM1A, rabbit anti-FLAG, mouse anti-FLAG clone M2 and rabbit anti-myosin IIA (Sigma); rabbit anti-Par3 (Upstate); rat anti-hemagglutinin (HA) clone 3F10 and mouse anti-GFP (Roche Diagnostics); mouse anti-HA clone 16B12 and mouse anti-GST clone 4C10 (Covance); rat anti-GFP (Nakarai); rabbit anti-GFP (MBL); Alexa Fluor 488-, 555-, 594- or 647-conjugated secondary antibody (Molecular Probes); Cy3-conjugated anti-rat IgG (Chemicon); Cy2- or peroxidase-conjugated anti-rat IgG (Jackson); and peroxidase-conjugated anti-mouse or anti-rabbit IgG (GE Healthcare).

Pull-down assay
Mouse E9.5 embryos were homogenized in a lysis buffer consisting of 20 mM Tris-HCl (pH 7.5) containing 0.5% Triton X-100, 150 mM NaCl, 1 mM EDTA, 5% glycerol, 1 mM PMSF, a protease inhibitor cocktail (Roche Diagnostics) and 1 mM dithiothreitol, and centrifuged at 15,000 *g* for 10 minutes. The supernatant was precleared with glutathione-sepharose 4B beads at 4°C for 1 hour, and then incubated with the glutathione-sepharose

4B beads loaded with GST-tagged ASD2 at 4°C for 2 hours. After washing the beads, the bound proteins were subjected to SDS-PAGE followed by silver staining using a Silver Stain MS kit (Wako).

Immunoprecipitation and western blotting
Cells were lysed at 4°C for 20 minutes in a lysis buffer consisting of 50 mM Tris-HCl (pH 7.5), containing 1% Nonidet P-40, 150 mM NaCl, 0.5 mM EDTA, 0.5 mM EGTA, 1.5 mM $MgCl_2$, a protease inhibitor cocktail (Roche Diagnostics) and 1 mM dithiothreitol. After centrifugation, the supernatants were incubated with the appropriate antibodies at 4°C for 2 hours. Then protein G-Sepharose beads (GE Healthcare) were added and incubation was continued for an additional 30 minutes. After washing the beads, bound proteins were subjected to SDS-PAGE and then western blotting. Signals on the bots were detected by using the ECL or ECL Plus detection system (GE Healthcare).

Cell culture and transfection
Madin-Darby canine kidney epithelial cells (MDCK, strain II) and COS7 cells were grown in a 1:1 mixture of DMEM and Ham's F12 medium supplemented with 10% fetal bovine serum (FBS). MDCK Tet-Off cells were purchased from BD Biosciences and maintained in DMEM supplemented with 10% tetracycline-free FBS, 1 µg/ml puromycin and 1 µg/ml doxycycline. MDCK or MDCK Tet-Off Cells were transfected with expression plasmids by using Lipofectamine 2000 (Invitrogen). For isolating their stable transfectants, transfected cells were selected and maintained in culture medium containing 200-400 µg/ml of Hygromycin B. COS7 cells were transfected by using Effectene transfection reagents (Qiagen).

Immunofluorescence microscopy for cultured cells
Cells grown on cover glasses were fixed with cold methanol at –20°C for 5 minutes, or with 4% (w/v) paraformaldehyde at room temperature for 20 minutes, and then made permeable with 0.5% Triton X-100 in Ca^{2+}- and Mg^{2+}-free phosphate- buffered saline (PBS). The cells were blocked with 10% (w/v) skim milk in PBS containing 0.1% Triton X-100 (PBS-T), and incubated at room temperature for 2 hours with primary antibodies in PBS-T containing 1% skim milk. After washes, the cells were incubated for 1 hour with fluorescence-labeled secondary antibodies, and subsequently mounted with FluoroSave (CalbioChem). The images were obtained by using a laser-scanning confocal microscope LSM510 (Carl Zeiss) equipped with a Plan Apochromat 63×/1.4 lens (Carl Zeiss). The measurement of apical junctional length and areas were performed by using an LSM4 image browser.

Manipulation of chicken embryos
Fertilized hens' eggs were purchased from Shiroyama Farm (Kanagawa, Japan) and incubated at 38.5°C to the desired stages. For chemical treatments and electroporation experiments, we used the modified New culture method, as described (Nakazawa et al., 2006). Electroporation was performed with an Intracel electroporator (Intracel) at the following setting: 6 volts, 3 pulses for 50 ms at a 200 ms interval.

For immunohistochemical studies, whole chicken embryos were fixed for 1 hour with 4% PFA in PBS containing 1 mM EGTA at 4°C. After replacement of the fixative with 30% sucrose, the embryos were frozen in OCT compound (Sakura Finetek). Sections of 10 µm were prepared with a cryostat, air-dried for 3 hours and stored. Rehydrated sections were treated with 0.3% Triton X-100 and 0.2% bovine serum albumin (BSA) in TBS for 10 minutes at room temperature, and then blocked at room temperature for 2 hours in a solution of 3% BSA and 10% goat serum in TBS. The sections were subsequently incubated for 2 hours with primary antibodies in a solution of 0.1% Triton X-100, 0.2% BSA and 1% goat serum in TBS at room temperature. After washing, the sections were incubated at room temperature for 1 hour with fluorescence-labeled secondary antibodies, and mounted in FluoroSave. Microscopic images were obtained by using an Axioplan2 microscope (Carl Zeiss).

For whole-mount preparations, neural tubes were dissected, cut at the ventral midline and fixed with 4% PFA in PBS at room temperature for 15 minutes. Then the neural tubes were blocked at room temperature for 2 hours in a solution containing 3% BSA, 10% goat serum and 0.5% Triton X-100 in TBS, after which they were incubated with primary antibodies in Can Get

Signal immunostain solution B (TOYOBO) at room temperature for 2 hours. After washes, the samples were incubated with fluorescence-labeled secondary antibodies at room temperature for 1 hour. After more washes, the neural tubes were mounted with their inner side up in glycerol gelatin (Sigma). Microscopic images were obtained by using the Axioplan2 microscope or LSM510 META multiphoton confocal system (Carl Zeiss) equipped with a Plan Apochromat 63×/1.4 lens (Carl Zeiss).

To estimate the population of cells with rosette configuration in the neural plate, we selected cell clusters with a vertex formed by more than five cells on the following grounds: in the sheets of randomly packed cells, the majority of cells are arranged theoretically with three-cell vertices (Honda and Eguchi, 1980); in natural epithelial cell sheets, we can also occasionally detect four-cell vertices (see Fig. 1B as an example), but rarely five- or six-cell vertices. Thus, we defined the cell clusters with a vertex formed by more than five cells as 'rosettes' organized via non-random cell arrangement.

RESULTS
Shroom3 interacts with Rock1 and Rock2 via the ASD2 domain
To affirm the role of the Shroom3 ASD2 domain in epithelial constriction in our experimental system, we constructed a FLAG-tagged full-length Shroom3 (Shrm-Full) or its mutant lacking the ASD2 domain (Shrm-ΔASD2; Fig. 1A), introduced these constructs into MDCK Tet-Off cells, the expression of which was controlled by the Tet-Off promoter, and isolated their stable transfectants. Without Shrm-Full expression in the presence of doxycycline, a suppressor of expression, the apical cell-cell boundaries delineated by immunostaining for ZO-1, a tight-junction protein, appeared slightly curved and/or serrated (Fig. 1B). When Shrm-Full was expressed by removal of doxycycline, the apical junctions of the transfectants became tense and straightened (Fig. 1B). By contrast, expression of Shrm-ΔASD2 had no such effects on the junctional morphology (Fig. 1B), confirming previous observations (Dietz et al., 2006).

To explore the function of the ASD2 domain (ASD2), we screened for molecules interacting with this domain by conducting pull-down assays. GST-tagged ASD2 (GST-ASD2) was incubated with a whole lysate of E9.5 mouse embryos, and the co-precipitated materials were analyzed by silver staining. The results showed that a protein of about 160 kDa interacted specifically with GST-ASD2 (see Fig. S1 in the supplementary material). Mass spectrometric analysis of this band showed that it contained the Rho kinases Rock1 and Rock2. To test the significance of this result, we incubated GST-ASD2 with a MDCK cell lysate, analyzed the co-precipitated materials by western blotting with anti-ROCK antibodies, and detected both Rock1 and Rock2 in this sample (Fig. 1C). Then, we examined whether the interactions between ASD2 and Rock1 or Rock2 also occurred in cells: FLAG-tagged ASD2 was co-expressed with either HA-tagged Rock1 or Rock2 in COS7 cells. Immunoprecipitates collected with anti-FLAG antibody from these cells contained both Rock1 and Rock2 (Fig. 1D). These results indicate that the ASD2 domain of Shroom3 interacted with Rock1 and Rock2.

Recruitment of ROCKs to the apical cell junctions by Shroom
To examine whether the distribution of ROCKs in cells could be regulated by Shroom3, we immunostained MDCK cells inducibly expressing Shroom3 with anti-Rock1 antibody. In the absence of expression of exogenous Shroom3, we detected only diffuse Rock1 signals distributed in the cytoplasm (Fig. 2A, upper), although its faint signals were occasionally detected emanating from cell-cell junctions. When the expression of Shroom3 was induced, Rock1 became condensed along the apical junctions; and its signals were
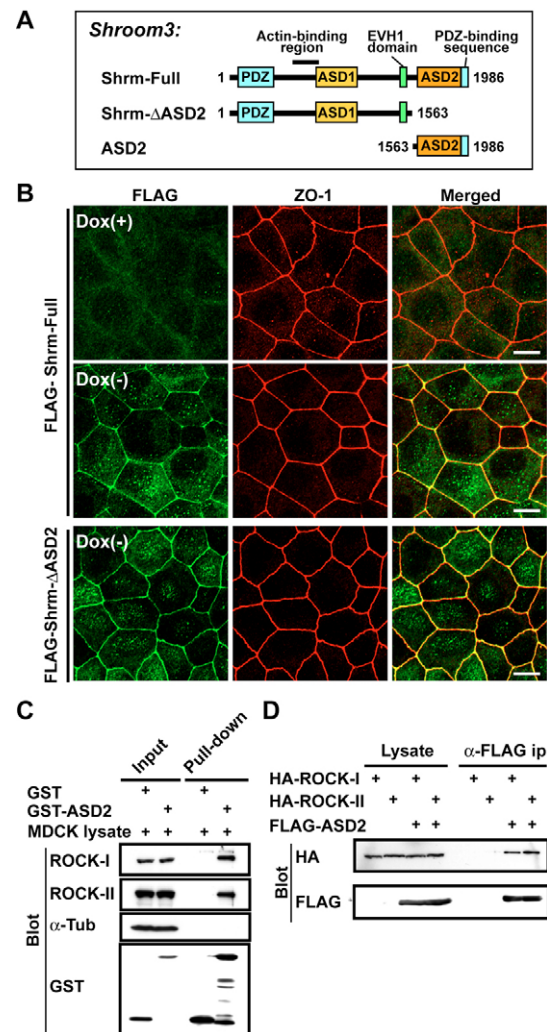

Fig. 1. Shroom3 binds ROCKs via its ASD2 domain. (**A**) Schematic representation of Shroom3 and its deletion mutants. (**B**) MDCK-Tet-Off cell lines inducibly expressing FLAG-tagged, full-length Shroom3 (Shrm-Full) or Shroom3-ΔASD2 (Shrm-ΔASD2) were double-immunostained for FLAG and ZO-1. Expression of these molecules is suppressed in the presence of doxycycline [Dox(+)], but induced by its removal (Dox[-]) from the culture medium. The apical cell junctions, delineated by ZO-1 signals, are tightened by expression of Shrm-Full but not of Shrm-ΔASD2. Scale bars: 10 μm. (**C**) In vitro interaction of ASD2 with endogenous Rock1 or Rock2. GST-tagged Shrm-ASD2 or GST was incubated with a MDCK cell lysate, and then pulled down with Glutathione-Sepharose 4B beads, followed by immunoblotting with antibodies against Rock1, Rock2, α-tubulin and GST. (**D**) In situ interaction of ASD2 with Rock1 or Rock2. COS7 cells were co-transfected with FLAG-tagged Shrm-ASD2 and HA-tagged Rock1 or Rock2. Cell lysates were subjected to immunoprecipitation with anti-FLAG antibody, followed by immunoblotting with anti-HA or anti-FLAG antibody.

colocalized with those of Shroom3 (Fig. 2A, middle). However, the expressed Shrm-ΔASD2 had no such effects on Rock1 distribution (Fig. 2A, bottom). We also introduced HA-tagged Rock2 into MDCK cells, and found that this construct was localized at the apical junctions only when Shroom3 was expressed (data not shown). Then, we tested whether Shrm-Full and Shrm-ΔASD2 were associated with endogenous ROCKs, and found that Rock1 and, to a lesser extent, Rock2 were co-immunoprecipitated with Shrm-Full,

but not with Shrm-ΔASD2, in the lysates of the above MDCK transfectants (Fig. 2B). All these results demonstrate that Shroom3 recruited ROCKs to the apical junctions by their ASD2 domain.

The Shroom-binding region on ROCKs antagonizes Shroom actions

In order to examine the role of the Shroom-ROCK interactions in epithelial junction constriction, we sought to determine the Shroom3-binding domains on Rock1 and Rock2. As both ROCKs gave similar results, we describe below only the results on Rock2 (see Fig. S2 in the supplementary material for the results on Rock1). We constructed various deletion mutants of Rock2, and examined their interaction with ASD2 by immunoprecipitation (Fig. 3A). None of the known domains on Rock2 interacted with ASD2. However, a central region located between the kinase and Rho-binding domains did strongly interact with it (Fig. 3A). We designated this Shroom3-binding region as RII-C1 (RI-C1 for Rock1). When EGFP-tagged RII-C1 was introduced into Shroom3-expressing MDCK Tet-Off cells, these peptides simply diffused in

the cytoplasm in the absence of Shroom3; whereas, in its presence, some of the expressed constructs became accumulated along the apical cell junctions together with Shroom3 (Fig. 3B, arrows). As a control, we used two constructs, termed RII-C2 and RII-C3, corresponding to the C-terminal half regions of Rock2, which had no ability to interact with Shroom3 (Fig. 3A), and found that these peptides were never localized at cell junctions even in the presence of Shroom3 (Fig. 3B; data not shown for RII-C3). We also noticed that the cells expressing RII-C1 exhibited broader surface areas compared with those not expressing RII-C1, as confirmed by quantitative measurement. Furthermore, the RII-C1-expressing cells tended to lose the Shroom3-mediated tension (Fig. 3B). Again, RII-C2 expression had no such effects. RI-C1 showed the activity comparable with that of RII-C1 (see Fig. S2 in the supplementary material).

The above results suggest that the C1 region of ROCKs competed with endogenous ROCKs for their interactions with Shroom3. To further test this possibility, we introduced EGFP-tagged RII-C1 or EGFP into MDCK Tet-Off Shroom3 transfectants, and then immunoprecipitated Shroom3 from these cells. The results showed that, when RII-C1 had been expressed, the co-immunoprecipitation of Rock1 with Shroom3 was greatly suppressed (Fig. 3C, left). In addition, we immunostained these cells with anti-Rock1 antibody. In contrast to the junctional accumulation of endogenous Rock1 in the Shroom3 transfectants without RII-C1, those expressing RII-C1 lost the junctional Rock1 signal (Fig. 3C, middle). The activation of ROCKs is known to lead to the phosphorylation of myosin regulatory light chains (MLCs), and this phosphorylation is crucial for the activation of myosin 2 (Riento and Ridley, 2003). In Shroom3-expressing MDCK Tet-Off cells, MLC phosphorylation was observed along the apical junctions, as described earlier (Hildebrand, 2005). However, when RII-C1 was expressed, MLC phosphorylation at these sites was significantly reduced (Fig. 3C, right). These results demonstrate that RII-C1 antagonized the interaction of endogenous ROCKs with Shroom3, resulting in the suppression of the tension-producing functions of Shroom3.

The Shroom3-Rock1 interaction is crucial for neural tube closure

To explore the role of the Shroom3-ROCK interaction in embryos, we first observed their distributions in the developing chicken neural tube, choosing the head regions at stages 9. As reported for other species (Hildebrand, 2005), Shroom3 was concentrated along the apical junctional area of the neuroepithelial cells. By using antibodies generated against the chicken Rock1, we found this molecule to be also condensed along the apical surface of the neural tubes, well colocalizing with Shroom3 (Fig. 4A). Phosphorylated myosin light chain (pMLC) was also colocalized with the apical junctional signals of Shroom3 and Rock1 (see below).

To study the functional and spatial relationships of these molecules, we constructed RNAi vectors specific for chicken Shroom3, as well as control vectors. To evaluate the knockdown effect of these vectors, we transfected MDCK cells with the Shroom3-specific RNAi vector, RNAi vector for the scrambled sequence of Shroom3 RNAi (control RNAi) or empty vector, together with an EGFP-tagged chicken Shroom3 central region (ch-Shrm/M, which contains the Shroom3 RNAi sequence) or EGFP. By western blotting of the transfected cell lysates, we found that the Shroom RNAi vector suppressed the expression of EGFP-ch-Shrm/M, but not that of EGFP (Fig. 4B). Neither of the control RNAi nor empty vectors affected the expression of either EGFP-ch-Shrm/M or EGFP.
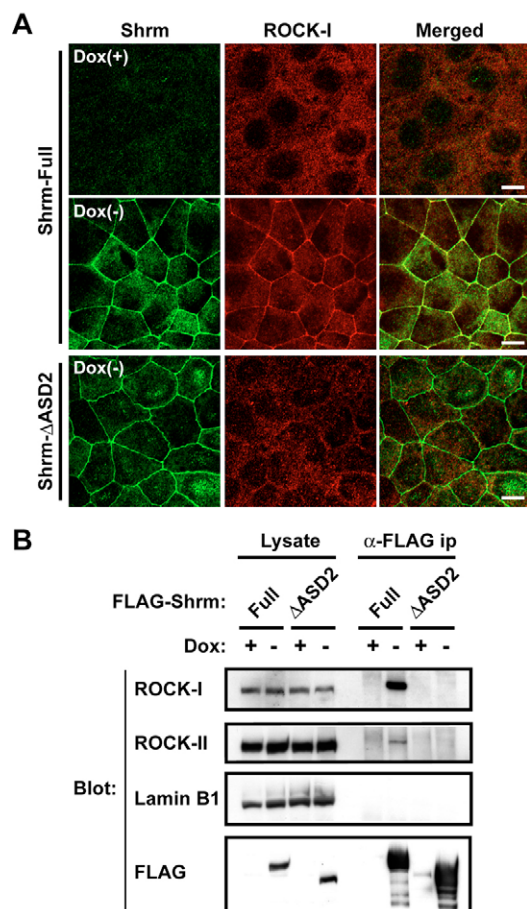

Fig. 2. Shroom3 recruits endogenous ROCK to the apical cell junctions in an ASD2-dependent way. (**A**) Localization of endogenous Rock1 in MDCK-Tet-Off cells expressing FLAG-tagged Shrm-Full or Shrm-ΔASD2. Endogenous Rock1 is visible along the apical cell junctions only in the presence of Shrm-Full [Dox(-)]. Scale bars: 10 μm. (**B**) Interaction of endogenous Rock1 or Rock2 with Shroom3 in cells. Lysates of the above cells were subjected to immunoprecipitation with anti-FLAG antibody, and then immunoblotted with antibodies against Rock1, Rock2, Lamin B1 and FLAG.
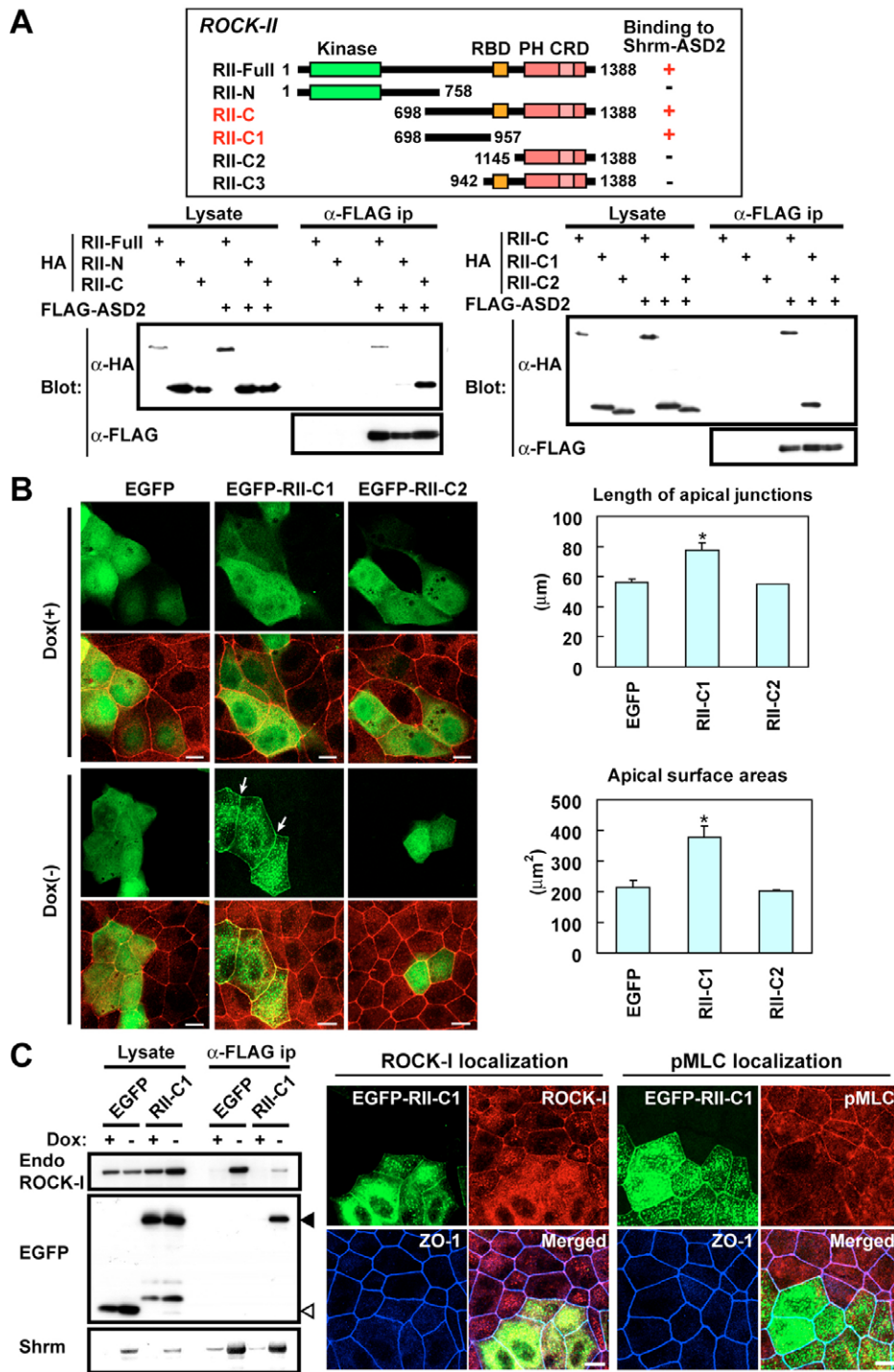
Fig. 3. A central fragment of ROCK interacts with ASD2, and can antagonize the endogenous ROCK-Shroom3 interaction. (**A**) (Top) Schematic representation of Rock2 and its deletion mutants. (Bottom) Interaction of ASD2 with Rock2 deletion mutants. COS7 cells were co-transfected with FLAG-tagged ASD2 and HA-tagged Rock2 (RII-Full) or its deletion mutants. Cell lysates were subjected to immunoprecipitation with anti-FLAG antibody, followed by immunoblotting with anti-HA or anti-FLAG antibody. Only the constructs containing the region from amino acids 698 to 957 can bind ASD2. See Fig. S2 in the supplementary material for the corresponding experiments for Rock1. (**B**) Expression of the central region of Rock2 (RII-C1) interferes with the action of Shroom3. EGFP-tagged RII-C1 or RII-C2 was expressed in MDCK-Tet-Off Shroom3 transfectants. The apical junctions were visualized with anti-ZO1 antibody (red). RII-C1 (green) is localized at the junctions only when Shroom3 expression has been induced by Dox(-), as indicated by arrows. Bar graphs show quantitative measurement of the length of apical junctions and apical surface areas in the same cultures. A total of 100-200 of GFP-positive cells were counted. Histograms are the average of three independent experiments, and bars represent the standard deviation. *$P<0.01$ against the EGFP-transfected cells. P-values were analyzed by Student's t-test throughout the manuscript. (**C**) RII-C1 interferes with the ROCK–Shroom3 interaction. (Left) MDCK-Tet-Off FLAG-Shrm-Full transfectants were further transfected with either EGFP-tagged RII-C1 or EGFP. From their lysates, Shroom3 was immunoprecipitated with anti-FLAG antibody, which was followed by detection of endogenous Rock1 or EGFP. Black triangle, EGFP-RII-C1; white triangle, EGFP. (Right) Localization of endogenous Rock1 or pMLC in Shroom3-expressing cells, in which restricted cells had been transfected with EGFP-RII-C1. Junctional localization of those molecules is inhibited in the RII-C1-positive cells. Scale bars: 10 μm.

Then, we transfected the future neural plate with these vectors by electroporation. Stage 3 chicken embryos were electroporated at the regions anterior to the primitive streak with a mixture of the RNAi vectors and EGFP-vector as a transfection marker, as illustrated in Fig. S3 in the supplementary material. Electroporated embryos were cultured for about 1 day, and fixed at stage 9. In embryos electroporated with the empty or control RNAi vector, not only Shroom3 but also Rock1 and pMLC remained localized at the apical surface of the neural tube (Fig. 4C, top and bottom rows). By contrast, in those electroporated with the Shroom3 RNAi vector, in which Shroom3 immunoreactive signals disappeared from the apical

surface of the neural tube, the Rock1 signals were also decreased at the apical region, although its diffuse cytoplasmic signals remained (Fig. 4C, middle row). In addition, the apical signals for MLC phosphorylation were also reduced. In these Shroom3 RNAi-electroporated embryos, the neural plate failed to bend normally, except at the floor plate, and did not close, suggesting that the inner constriction of the tube was defective, as observed for other species (Haigo et al., 2003; Hildebrand and Soriano, 1999). Importantly, the distribution of ZO-1 delineating the apical surface of the neural tube was almost the same among these electroporated embryos, suggesting that the apical surface structures were not particularly
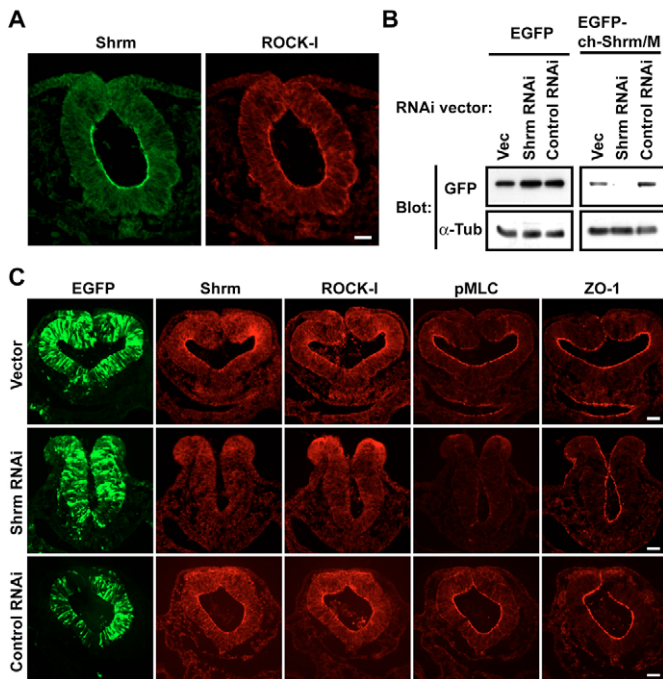
Fig. 4. Depletion of Shroom3 abolishes the apical localization of Rock1 in the neural tube. (**A**) Co-localization of Shroom3 and Rock1 at the apical junctions of chicken neural tubes. A transverse section of stage 9 chicken embryo at the hindbrain level was double-immunostained for these proteins. (**B**) Test for RNAi-mediated depletion of chicken Shroom3. MDCK cells were co-transfected with RNAi vectors for the chicken Shroom3 (Shrm RNAi), scrambled sequences (Control RNAi) or empty vector (Vec), and with either an EGFP-tagged middle region of chicken Shroom3 (EGFP-ch-Shrm/M) or EGFP alone. The cell lysates were immunoblotted with anti-GFP or anti-α-tubulin antibodies. There is effective and specific depletion of Shroom3 by the RNAi vector. (**C**) Effects of Shroom3 knockdown on the localization of Rock1 in the neural tube. Chicken embryos were co-electroporated with EGFP and RNAi vectors, as shown in Fig. S3 in the supplementary material, and fixed at stage 9. A section of an embryo at the forebrain-midbrain level was double-immunostained for EGFP and Shroom3, and adjacent sections were immunostained for Rock1, pMLC and ZO-1 in each experiment. Rock1 and pMLC levels are reduced at the apical junctions in the Shroom3-depleted tube (Shrm RNAi), the closure of which is also perturbed. Scale bars: 20 μm.

distorted by the electroporation. These results suggest that Shroom3 recruited Rock1 to the apical junctions of the neural tube, leading to the phosphorylation of MLC, and that this process was important for neural tube closure.

To test directly the role of the Shroom3-Rock1 interaction in neural tube morphogenesis, we electroporated embryos with the expression vector for EGFP-tagged RII-C1, by the same methods as described above. As negative controls, we used EGFP or EGFP-tagged RII-C2. Although the expression of these control vectors had no effects on neural tube development, that of EGFP-RII-C1 reduced the apical accumulation of both Rock1 and pMLC in the neural tube (Fig. 5). Concomitantly, these RII-C1-treated tubes failed to bend, and consequently could not close, as observed in the Shroom3 RNAi-electroporated embryos. These results strongly suggest that RII-C1 interfered with the interactions between Shroom3 and ROCK also in vivo, leading to the malformation of the neural tube.
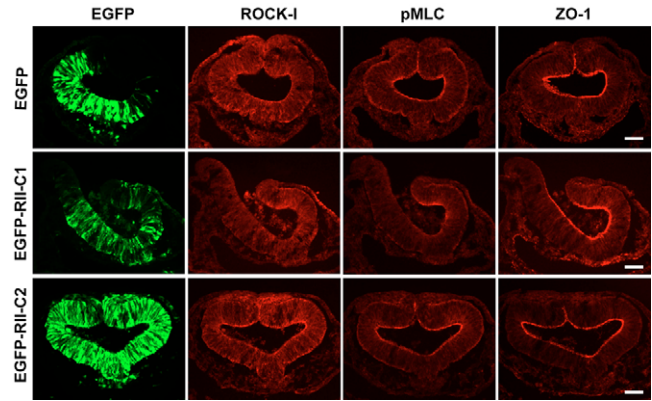

Fig. 5. Expression of RII-C1 in the neural tube antagonizes the apical localization of Rock1 as well as tube closure. Chicken embryos were electroporated with the expression vectors for EGFP, EGFP-tagged RII-C1 or EGFP-tagged RII-C2, and fixed at stage 9. A section of an embryo at the forebrain-midbrain level was double-immunostained for EGFP and Rock1, and adjacent sections were immunostained for pMLC and ZO-1 in each experiment. The neural tube fails to close at the side where the transfection of RII-C1 was more efficient. In this region, the apical levels of Rock1 and pMLC are downregulated. Scale bars: 20 μm.

Cell-level analysis of ROCK-dependent neural tube closure

The processes of neural plate invagination have not been fully analyzed with regard to cell behavior in the 2-dimensional neuroepithelial plane. For understating of the role of Shroom3 and ROCKs in neural tube closure at the cellular level, we decided to observe the morphology of individual neuroepithelial cells at their apical surfaces: we dissected the tubes from embryos at stages 8 to 9 when neural tube closure is proceeding, opened them by cutting along the dorsal midline, and then immunostained them for various markers (Fig. 6A). As the morphology of the cells comprising the neural tube varies to some extent with the region of the tube, we selected the lateral wall of the midbrain for our most detailed analysis, excluding the areas proximate to the dorsal and ventral midlines.

ZO-1 immunostaining, which delineates the neuroepithelial cell-cell junctions at their apical-most region, showed that cell morphology and assembly pattern in the closing tubes was complex at first glance (Fig. 6B). Close examinations of these samples, however, suggested that some order existed within the cell arrangement. For example, a cluster of cells often displayed a rosette-like arrangement with condensed ZO-1 signals at their vertex points (Fig. 6B,E, dotted circles), which was reminiscent of that observed in epithelial layers undergoing cell intercalation in *Drosophila* embryos (Blankenship et al., 2006). Some other cells were arranged in an arch-like or oval pattern (Fig. 6B,E, dotted oval). Along these ZO-1 signals, pMLC immunosignals displayed unexpected distributions (Fig. 6B): the pMLC signals were detected only at restricted cell-cell boundaries. These signals on an individual cell were often contiguous to those on the neighboring cells, resulting in a linear extension of the signals over four or five cells or even more (Fig. 6B). Intriguingly, these linear pMLC signals tended to be oriented along the dorsoventral axis of the embryo, although not absolutely (Fig. 6C). Other pMLC signals were punctate and concentrated at the converged or vertex points of the rosette-forming cells described above, although the signals

at a vertex were sometimes continuous to the above linear pMLC signals. To quantify the ratio of cell clusters assuming such rosette configuration, we counted the cells organizing a cluster in which six cells and more were radially converged on a pMLC-condensed center (see Materials and methods for the criteria for this scoring) and found that 30.8±5.1% (the mean±s.d.; 127-250 cells were counted per sample, n=3) of the neuroepithelial cells composing the midbrain lateral wall in stage 9 embryos displayed this configuration. We also counted the vertices, at which six cell-cell borders or more meet; and estimated that 17.0±4.2% (the

mean±s.d.; 156-275 vertices were counted per sample, n=3) of the vertices had this configuration. Stage 8 embryos gave similar values.

When myosin IIA was immunostained, this protein was distributed along all apical cell-cell boundaries, colocalizing with ZO-1 (see Fig. S4 in the supplementary material). This means that only the phosphorylation level of MLC in the myosin II was locally upregulated in the above samples. Par3, another apical junction marker, was also ubiquitously distributed (see Fig. S4 in the supplementary material). Immunoreactive signals for Shroom3 were

Fig. 6. Cell arrangement and pMLC distribution at the apical surface of the neural tube. (**A**) Preparation of flat-mount samples to observe the inner (apical) surface of the neural tube in stage 8-9 chicken embryos. The midbrain areas, marked with dotted squares, were selected for the observations. DM, dorsal midline; VM, ventral midline. In all the images shown below, the dorsal side is at the top and the anterior side is towards the left. (**B**) Double-immunostaining for ZO-1 and pMLC at the apical surface of the neural tube in stage 8 embryos. Representative cell clusters with rosette-like arrangement, where pMLC is concentrated at the central regions, are encircled; and those with arch-type arrangement are marked by an oval. Arrows indicate examples of linearly arranged pMLC signals. A-P, anteroposterior axis; D-V, dorsoventral axis. Scale bar: 10 μm. (**C**) The angular distribution of linear pMLC signals on the apical surface of neural tubes. Linear pMLC signals of more than 10 μm (68-89 signals/field) from four different fields from four embryos at stage 8-9 were analyzed for length and orientation. Horizontal and vertical axes represent the anterior-posterior and dorsal-ventral orientations, respectively. Percentages of the signals oriented at the angles between 0° and 30°, 30° and 60°, and 60° and 90° to the anterior-posterior axis were calculated. pMLC signals are more abundant along the dorsoventral axis. (**D**) Double immunostaining for Shroom3 and ZO-1 or pMLC at the apical surface of the neural tube in stage 9 embryos. ZO-1 colocalizes with Shroom3, whereas pMLC colocalizes only with restricted Shroom3 signals. (**E**) Effects of Y27632 on the distribution of pMLC and cell morphology. Stage 8(–) embryos (with two or three somites) were incubated in the presence of Y27632 (100 μM) or 1% DMSO (control) in the culture medium for 6 hours prior to fixation, and their neural tubes were double-immunostained for pMLC and ZO-1. Examples of rosette-like and arched cell clusters are marked with a circle and oval, respectively. When rosette is defined as a cluster comprising six cells or more, in which the cells radially converged on a constricted point, cell clusters with such configuration are undetectable in the Y27632-treated sample shown. The bar graphs show the length of apical junctions, apical surface areas and percent of cells with pMLC signals. All the cells in randomly selected fields (105-250 cells/field) were measured. Histograms are the average of three different fields from three embryos, and bars represent the standard deviation. *P<0.05; **P<0.01 against 1% DMSO-treated embryos. Scale bars: 10 μm.
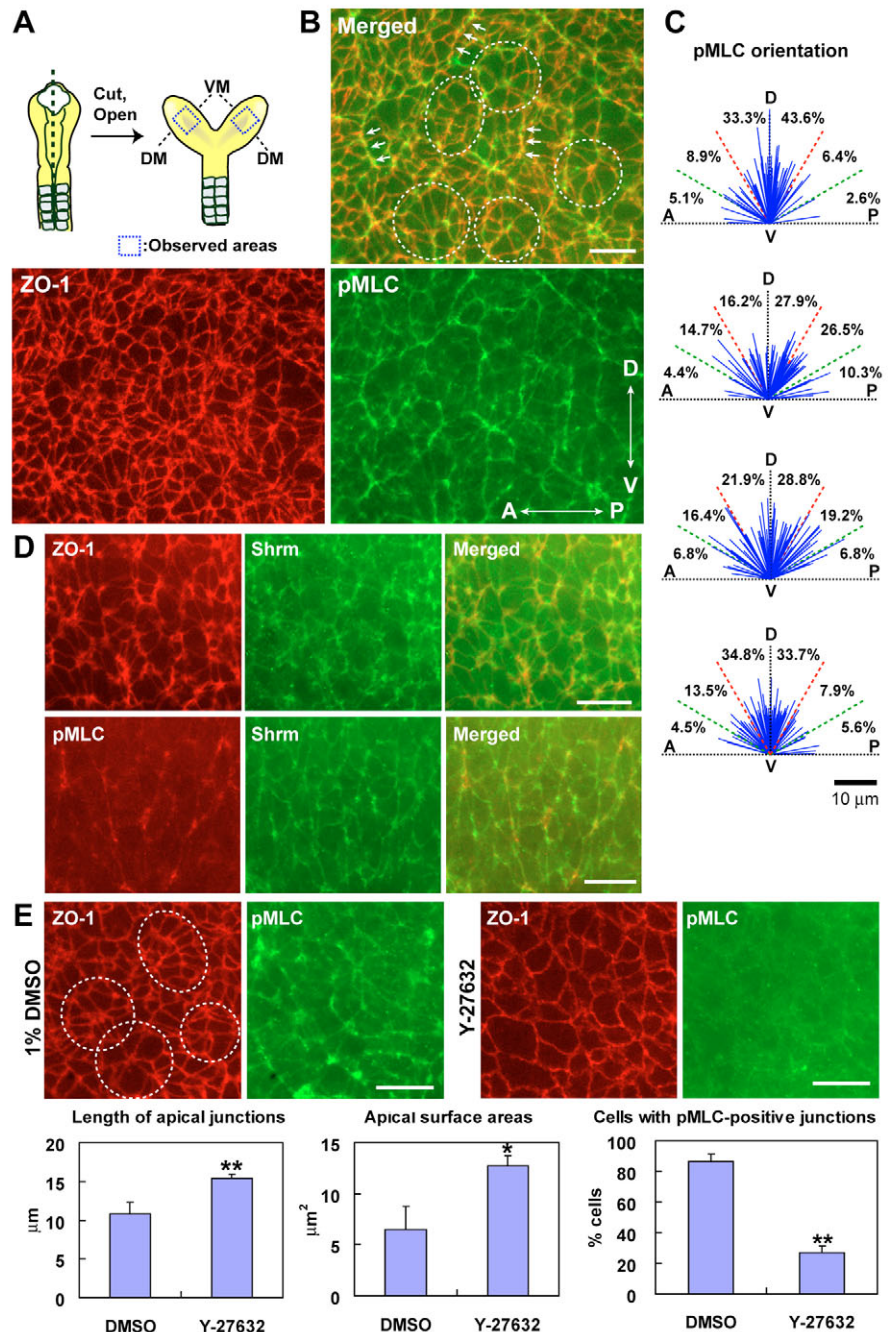
faint in these whole-mount preparations, preventing us from detailed analysis of its distribution; nevertheless, the immunostaining results suggested that Shroom3 was localized along all the ZO-1 positive cell-cell boundaries (Fig. 6D). When pMLC and Shroom were double-stained, they were found to be colocalized, but pMLC was detected only in a subpopulation of the Shroom-positive cell-cell boundaries (Fig. 6D), as expected from the above observations. Signals for Rock1 were even fainter, not allowing us to conduct its immunolocalization analysis in the whole-mount samples (data not shown).

For comparison, we also examined the dorsal ectoderm in embryos at the stages prior to neural plate invagination (see Fig. S4 in the supplementary material). Some of the ectodermal cells also showed the rosette configuration. pMLC was more or less detected throughout the apical cell-cell boundaries, and it tended to be concentrated at the vertex regions including the center of rosettes. However, these pMLC signals were not arranged so as to extend over multiple cell-cell boundaries, suggesting that the above-described profile of pMLC localization developed during the invagination of the neural plate.

To test whether ROCK signals played any role in the above arrangements of neural tube cells, we added Y27632, a ROCK inhibitor, to the culture medium of embryos at 6 hours prior to the fixation at stage 9. As reported earlier (Wei et al., 2001), this inhibitor completely blocked neural tube closure. Double immunostaining for ZO-1 and pMLC showed that pMLC signals, whether linear or punctate, were drastically diminished; and, simultaneously, the apical surface of individual neural tube cells was significantly expanded (Fig. 6E). In these Y27632-treated neural plates, cells with the rosette configuration became less frequent; i.e. the vertices consisting of more than five cell-cell borders were reduced to $4.9\pm3.0\%$ (the mean $\pm$ s.d.; 152-202 vertices were counted per sample, $n=3$) of the total vertices in the neural plate region shown in Fig. 6E; this value was originally 17% in the untreated samples (see above). These results suggest that ROCK signals are crucial for the rosette-type arrangement of neuroepithelial cells in the two-dimensional plane.

Blocking of the Shroom-ROCK interactions perturbs planar cell arrangement in the neural tube

To finally examine whether the above actions of ROCK on neuroepithelial cells depended on the Shroom-associated pool of this molecule, we looked at the effects of RII-C1 expression in the neural tube on cell arrangement, as well as on pMLC localization. Embryos electroporated with the expression vector for EGFP, EGFP-tagged RII-C1 or RII-C2, as described for the experiments for Fig. 5, were triple-immunostained for EGFP, pMLC and ZO-1. These vectors were expressed in a mosaic fashion in the neuroepithelial layer. Analysis of the layers densely transfected with these vectors showed that RII-C1 expression resulted in a significant reduction in the pMLC-bearing cells (Fig. 7), consistent with the results obtained with tissue sections. Moreover, cells that had lost pMLC in the RII-C1-expressing layer also lost the typical rosette configuration, although residual pMLC signals, when detectable, still localized at the convergent points of cells (Fig. 7, arrows). EGFP and RII-C2, however, showed no such effects. These results support the idea that the Shroom-ROCK interaction is required not only for the local phosphorylation of junctional MLC but also for the specific two-dimensional arrangement of developing neural tube cells.
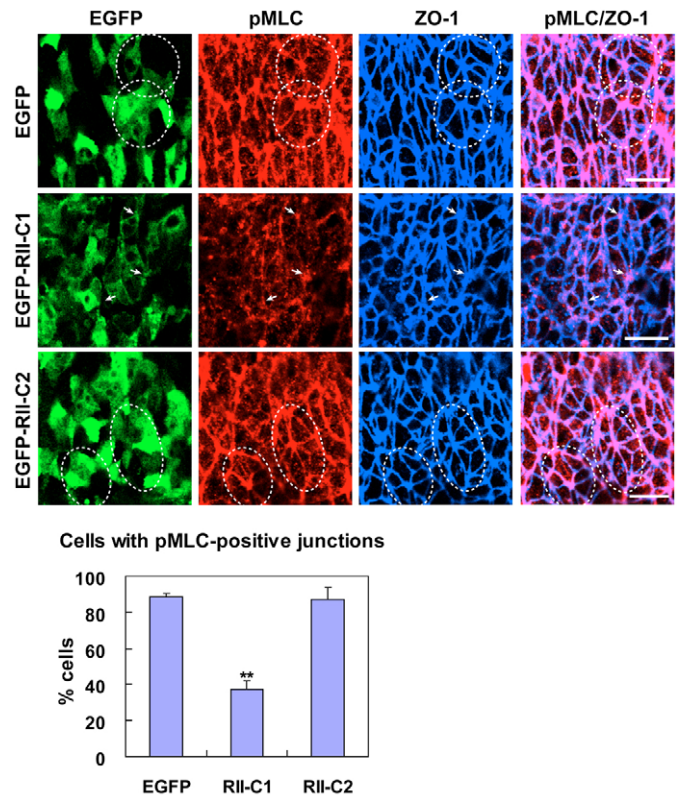

Fig. 7. Expression of RII-C1 disturbs cell arrangement at the apical surface of the neural tube. Confocal views of triple-immunostaining for EGFP, pMLC and ZO-1 at the apical surface of the neural tubes electroporated with EGFP, EGFP-tagged RII-C1 or RII-C2 and incubated as in the experiments for Fig. 5. Cells displaying the rosette configuration, which were defined as in Fig. 6E, are encircled. No such rosettes are detectable in the RII-C1-positive layer. Arrows indicate residual pMLC signals on which some cells converge, but not assuming the complete rosette configuration as defined above. The bar graph shows results of quantification of pMLC-positive cells. All EGFP-positive cells in randomly selected fields (30-102, 72-132 and 95-178 cells/field for RII-C1, RII-C2 and EGFP, respectively) were counted. Histogram is the average of three different fields from three chicken embryos, and bars represent the standard deviation. **$P<0.01$ against EGFP-transfected embryos. Scale bars: 10 μm.

DISCUSSION

Previous studies suggested that the Shroom3-dependent epithelial cell shape regulation was ROCK dependent (Hildebrand, 2005). Our present results have provided evidence that Shroom3 physically associated with ROCKs via the ASD2 domain. We also identified a Shroom3-binding region on Rock1 and Rock2. Peptides containing this region competed with endogenous ROCKs in their interaction with Shroom3, leading to the suppression of the junctional recruitment of ROCKs and a concomitant relaxation of the apical junctions. These results suggest that Shroom3 functions as a scaffold to recruit ROCKs to the apical junctional complex (AJC). How Shroom3 itself becomes localized at the AJC remains to be elucidated, although Shroom2 was earlier shown to interact with ZO-1 (Etournay et al., 2007).

ROCKs induce the contraction of actin fibers by phosphorylating MLC as well as by inhibiting myosin phosphatase (Riento and Ridley, 2003). We showed that the recruitment of ROCKs to the AJC well correlated with the phosphorylation of MLC localized at the

same sites in MDCK cells and that the ROCK inhibitor Y27632 suppressed the MLC phosphorylation at the corresponding sites in the neural tube. As the epithelial AJCs are lined with the circumferential actin belts, it is likely that, by being recruited to the AJC, the ROCKs directly control the contraction of these actin belts via the classic MLC phosphorylation pathway. In the absence of Shroom3, the amount of ROCKs at the AJC was only residual in MCDK cells and in the neural tube. These observations suggest that ROCKs may not be able to regulate the apical junction organization effectively without Shroom3 or other molecules having similar functions.

Neural tube closure is not only a Shroom-dependent process but also a ROCK-dependent one (Wei et al., 2001; Ybot-Gonzalez et al., 2007). We showed that the blocking of the Shroom3-ROCK interaction with RII-C1 suppressed neural tube closure, concomitantly downregulating MLC phosphorylation at the AJC. These findings strongly suggest that the Shroom3-dependent recruitment of ROCKs to the neuroepithelial AJC is crucial for the bending morphogenesis of neural tube. However, we suspect that simple constriction of the apical junctions in the neuroepithelial layer would not be sufficient for the control of its bending, as this process was polarized, occurring along the dorsoventral axis. Thus, to close the neural tube correctly, the ROCK-dependent contraction of neuroepithelial cell borders would need to be spatially regulated.

To understand the cellular basis of polarized neural tube closure, we analyzed the cell assembly pattern in the inner surface of the closing tube. The pattern was complex, and the apical morphology of cells extensively varied from cell to cell. Within the complexities, however, we could detect some order; that is, the rosette-like or arch-type arrangement of neuroepithelial cells. Rosette formation has been observed in *Drosophila* epithelial cells undergoing intercalation during the germ band extension of embryos (Blankenship et al., 2006). During this intercalation, the boundaries between the anterior and posterior cells become enriched in myosin 2; and other molecules such as Par3 complement this pattern by localizing along the other sides of the junction on the same cell (Bertet et al., 2004; Zallen and Wieschaus, 2004). Based on these observations, it is thought that the actomyosin-dependent contraction of the cell-cell borders oriented along the dorsoventral axis, coordinated with the concomitant expansion of the other cell boundaries towards the anterior-posterior axis, leads the cells to intercalate and that the rosette-like arrangement of cells represents an intermediate stage of this process (Blankenship et al., 2006). Our finding of rosettes suggests that vertebrate neuroepithelial cells may use similar strategy for regulation of cell rearrangement during the neural tube closure. This view is consistent with the observations that neural tube morphogenesis involves convergent extension of neuroepithelial cells (Ybot-Gonzalez et al., 2007).

In the chicken neuroepithelial layer, however, myosin 2 and Par3 were rather ubiquitously localized along the cell-cell junctions. Instead, pMLC distribution was polarized: pMLC was concentrated only at restricted sites on the AJC surrounding a cell, and this pMLC signal was often contiguous to that on the neighboring cells, thus resulting in a linear extension of pMLC signals over a group of cells. Moreover, these pMLC signals tended to be oriented along the dorsoventral axis of the neural tube. Other pMLC signals were concentrated around the center of rosettes. The role of these unique distributions of pMLC remains to be further explored, but we can imagine a scheme such that the cell-cell junctions with the linear pMLC may contract at subsequent developmental stages; the rosette configuration of cells could have been a consequence of the contraction of these junctions. Such form of cell rearrangement, if it occurs, is reminiscent of the cell intercalation processes observed in *Drosophila* germ band extension, although the underlying molecular mechanisms appear to have diverged between these species.

However, we observed that even the dorsal ectoderm prior to invagination exhibited similar rosettes, indicating that rosette formation was not specific to the closing neural tube. Cells in the dorsal ectoderm may also be intercalating, e.g. for the anterior-posterior elongation of the embryo, so this may explain why they also have rosettes. Hereby, we could consider another view for the roles of pMLC localization. It is possible that rosette formation is generally involved in cell intercalation and that the linear pMLC has a separate role. It is tempting to speculate that the linear pMLC with the dorsoventral orientation could be used for the contraction of a group of cell junctions along this axis, leading to the polarized bending of the neuroepithelial sheet, and that this type of pMLC localization could have been elaborated specifically for closing a tube. The ROCK inhibitor and RII-C1 peptides abolished these pMLC signals, as well as inhibited neural tube closure and rosette formation, suggesting that the Shroom-dependent recruitment of ROCKs to the AJC and the ROCK-dependent contraction of AJC are necessary for all of these cell rearrangement processes.

Finally, how can the MLC phosphorylation be upregulated locally under the ubiquitous distribution of myosin II along the AJCs? Although Sroom3 also appeared to be localized ubiquitously along the AJCs, pMLC was not always detected at the Shroom-positive junctions, suggesting that the association of MLC with the Shroom-ROCK complex was not sufficient for inducing MLC phosphorylation in the neural tube. Yet unidentified regulators may locally activate ROCKs, possibly through the upregulation of some RhoGEFs. Planar polarity genes expressed in the neural tube (Ybot-Gonzalez et al., 2007) may play a role in such regulation, because the local distribution of pMLC can be considered sort of planar polarity phenomenon. It was also suggested that the zebrafish Rho kinase 2 acts downstream of non-canonical Wnt11 signaling (Marlow et al., 2002). Identification of such local regulators for MLC phosphorylation is important to test the hypotheses proposed in this work.

Supplementary material
Supplementary material for this article is available at
http://dev.biologists.org/cgi/content/full/135/8/1493/DC1

References
Amano, M., Ito, M., Kimura, K., Fukata, Y., Chihara, K., Nakano, T., Matsuura, Y. and Kaibuchi, K. (1996). Phosphorylation and activation of myosin by Rho-associated kinase (Rho-kinase). *J. Biol. Chem.* **271**, 20246-20249.
Barrett, K., Leptin, M. and Settleman, J. (1997). The Rho GTPase and a putative RhoGEF mediate a signaling pathway for the cell shape changes in Drosophila gastrulation. *Cell* **91**, 905-915.
Bertet, C., Sulak, L. and Lecuit, T. (2004). Myosin-dependent junction remodelling controls planar cell intercalation and axis elongation. *Nature* **429**, 667-671.
Blankenship, J. T., Backovic, S. T., Sanny, J. S., Weitz, O. and Zallen, J. A. (2006). Multicellular rosette formation links planar cell polarity to tissue morphogenesis. *Dev. Cell* **11**, 459-470.
Copp, A. J., Greene, N. D. and Murdoch, J. N. (2003). The genetic basis of mammalian neurulation. *Nat. Rev. Genet.* **4**, 784-793.

Costa, M., Wilson, E. T. and Wieschaus, E. (1994). A putative cell signal encoded by the folded gastrulation gene coordinates cell shape changes during Drosophila gastrulation. *Cell* **76**, 1075-1089.

Dietz, M. L., Bernaciak, T. M., Vendetti, F., Kielec, J. M. and Hildebrand, J. D. (2006). Differential actin-dependent localization modulates the evolutionarily conserved activity of Shroom family proteins. *J. Biol. Chem.* **281**, 20542-20554.

Etournay, R., Zwaenepoel, I., Perfettini, I., Legrain, P., Petit, C. and El-Amraoui, A. (2007). Shroom2, a myosin-VIIa- and actin-binding protein, directly interacts with ZO-1 at tight junctions. *J. Cell Sci.* **120**, 2838-2850.

Fairbank, P. D., Lee, C., Ellis, A., Hildebrand, J. D., Gross, J. M. and Wallingford, J. B. (2006). Shroom2 (APXL) regulates melanosome biogenesis and localization in the retinal pigment epithelium. *Development* **133**, 4109-4118.

Farquhar, M. G. and Palade, G. E. (1963). Junctional complexes in various epithelia. *J. Cell Biol.* **17**, 375-412.

Hagens, O., Ballabio, A., Kalscheuer, V., Kraehenbuhl, J. P., Schiaffino, M. V., Smith, P., Staub, O., Hildebrand, J. and Wallingford, J. B. (2006). A new standard nomenclature for proteins related to Apx and Shroom. *BMC Cell Biol.* **7**, 18.

Haigo, S. L., Hildebrand, J. D., Harland, R. M. and Wallingford, J. B. (2003). Shroom induces apical constriction and is required for hingepoint formation during neural tube closure. *Curr. Biol.* **13**, 2125-2137.

Hildebrand, J. D. (2005). Shroom regulates epithelial cell shape via the apical positioning of an actomyosin network. *J. Cell Sci.* **118**, 5191-5203.

Hildebrand, J. D. and Soriano, P. (1999). Shroom, a PDZ domain-containing actin-binding protein, is required for neural tube morphogenesis in mice. *Cell* **99**, 485-497.

Honda, H. and Eguchi, G. (1980). How much does the cell boundary contract in a monolayered cell sheet? *J. Theor. Biol.* **84**, 575-588.

Kawano, Y., Fukata, Y., Oshiro, N., Amano, M., Nakamura, T., Ito, M., Matsumura, F., Inagaki, M. and Kaibuchi, K. (1999). Phosphorylation of myosin-binding subunit (MBS) of myosin phosphatase by Rho-kinase in vivo. *J. Cell Biol.* **147**, 1023-1038.

Kolsch, V., Seher, T., Fernandez-Ballester, G. J., Serrano, L. and Leptin, M. (2007). Control of Drosophila gastrulation by apical localization of adherens junctions and RhoGEF2. *Science* **315**, 384-386.

Lecuit, T. and Lenne, P. F. (2007). Cell surface mechanics and the control of cell shape, tissue patterns and morphogenesis. *Nat. Rev. Mol. Cell Biol.* **8**, 633-644.

Lee, C., Scherr, H. M. and Wallingford, J. B. (2007). Shroom family proteins regulate gamma-tubulin distribution and microtubule architecture during epithelial cell shape change. *Development* **134**, 1431-1441.

Marlow, F., Topczewski, J., Sepich, D. and Solnica-Krezel, L. (2002). Zebrafish Rho kinase 2 acts downstream of Wnt11 to mediate cell polarity and effective convergence and extension movements. *Curr. Biol.* **12**, 876-884.

Matsumura, F. (2005). Regulation of myosin II during cytokinesis in higher eukaryotes. *Trends Cell Biol.* **15**, 371-377.

Nakazawa, F., Nagai, H., Shin, M. and Sheng, G. (2006). Negative regulation of primitive hematopoiesis by the FGF signaling pathway. *Blood* **108**, 3335-3343.

Nikolaidou, K. K. and Barrett, K. (2004). A Rho GTPase signaling pathway is used reiteratively in epithelial folding and potentially selects the outcome of Rho activation. *Curr. Biol.* **14**, 1822-1826.

Parks, S. and Wieschaus, E. (1991). The Drosophila gastrulation gene concertina encodes a G alpha-like protein. *Cell* **64**, 447-458.

Perez-Moreno, M., Jamora, C. and Fuchs, E. (2003). Sticky business: orchestrating cellular signals at adherens junctions. *Cell* **112**, 535-548.

Pilot, F. and Lecuit, T. (2005). Compartmentalized morphogenesis in epithelia: from cell to tissue shape. *Dev. Dyn.* **232**, 685-694.

Riento, K. and Ridley, A. J. (2003). Rocks: multifunctional kinases in cell behaviour. *Nat. Rev. Mol. Cell Biol.* **4**, 446-456.

Rogers, S. L., Wiedemann, U., Hacker, U., Turck, C. and Vale, R. D. (2004). Drosophila RhoGEF2 associates with microtubule plus ends in an EB1-dependent manner. *Curr. Biol.* **14**, 1827-1833.

Sahai, E. and Marshall, C. J. (2002). ROCK and Dia have opposing effects on adherens junctions downstream of Rho. *Nat. Cell Biol.* **4**, 408-415.

Tepass, U., Tanentzapf, G., Ward, R. and Fehon, R. (2001). Epithelial cell polarity and cell junctions in Drosophila. *Annu. Rev. Genet.* **35**, 747-784.

Vogelmann, R. and Nelson, W. J. (2005). Fractionation of the epithelial apical junctional complex: reassessment of protein distributions in different substructures. *Mol. Biol. Cell* **16**, 701-716.

Walsh, S. V., Hopkins, A. M., Chen, J., Narumiya, S., Parkos, C. A. and Nusrat, A. (2001). Rho kinase regulates tight junction function and is necessary for tight junction assembly in polarized intestinal epithelia. *Gastroenterology* **121**, 566-579.

Wei, L., Roberts, W., Wang, L., Yamada, M., Zhang, S., Zhao, Z., Rivkees, S. A., Schwartz, R. J. and Imanaka-Yoshida, K. (2001). Rho kinases play an obligatory role in vertebrate embryonic organogenesis. *Development* **128**, 2953-2962.

Ybot-Gonzalez, P., Savery, D., Gerrelli, D., Signore, M., Mitchell, C. E., Faux, C. H., Greene, N. D. and Copp, A. J. (2007). Convergent extension, planar-cell-polarity signalling and initiation of mouse neural tube closure. *Development* **134**, 789-799.

Yoder, M. and Hildebrand, J. D. (2007). Shroom4 (Kiaa1202) is an actin-associated protein implicated in cytoskeletal organization. *Cell Motil. Cytoskel.* **64**, 49-63.

Zallen, J. A. and Wieschaus, E. (2004). Patterned gene expression directs bipolar planar polarity in Drosophila. *Dev. Cell* **6**, 343-355.